

Article

Dynamics and Control of Lateral Tower Vibrations in Offshore Wind Turbines by Means of Active Generator Torque

Zili Zhang ^{1,*}, Søren R. K. Nielsen ¹, Frede Blaabjerg ² and Dao Zhou ²

¹ Department of Civil Engineering, Aalborg University, Sofiendalsvej 11, 9200 Aalborg SV, Denmark; E-Mail: srkn@civil.aau.dk

² Department of Energy Technology, Aalborg University, Pontoppidanstraede 101, 9220 Aalborg East, Denmark; E-Mails: fbl@et.aau.dk (F.B.); zda@et.aau.dk (D.Z.)

* Author to whom correspondence should be addressed; E-Mail: zlz@civil.aau.dk; Tel.: +45-92-266-226.

External Editor: Simon J. Watson

Received: 6 July 2014; in revised form: 6 November 2014 / Accepted: 13 November 2014 /

Published: 21 November 2014

Abstract: Lateral tower vibrations of offshore wind turbines are normally lightly damped, and large amplitude vibrations induced by wind and wave loads in this direction may significantly shorten the fatigue life of the tower. This paper proposes the modeling and control of lateral tower vibrations in offshore wind turbines using active generator torque. To implement the active control algorithm, both the mechanical and power electronic aspects have been taken into consideration. A 13-degrees-of-freedom aeroelastic wind turbine model with generator and pitch controllers is derived using the Euler–Lagrangian approach. The model displays important features of wind turbines, such as mixed moving frame and fixed frame-defined degrees-of-freedom, couplings of the tower-blade-drivetrain vibrations, as well as aerodynamic damping present in different modes of motions. The load transfer mechanisms from the drivetrain and the generator to the nacelle are derived, and the interaction between the generator torque and the lateral tower vibration are presented in a generalized manner. A three-dimensional rotational sampled turbulence field is generated and applied to the rotor, and the tower is excited by a first order wave load in the lateral direction. Next, a simple active control algorithm is proposed based on active generator torques with feedback from the measured lateral tower vibrations. A full-scale power converter configuration with a cascaded loop control structure is also introduced to produce the feedback control torque in real time. Numerical simulations have been carried out using

data calibrated to the referential 5-MW NREL (National Renewable Energy Laboratory) offshore wind turbine. Cases of drivetrains with a gearbox and direct drive to the generator are considered using the same time series for the wave and turbulence loadings. Results show that by using active generator torque control, lateral tower vibrations can be significantly mitigated for both gear-driven and direct-driven wind turbines, with modest influence on the smoothness of the power output from the generator.

Keywords: offshore wind turbine; active generator control; lateral tower vibration; feedback control; aeroelastic model

1. Introduction

Modern multi-megawatt wind turbines are designed with increasingly larger rotors and higher towers, in order to capture more energy throughout their lifetime and, thereby, reduce the cost of energy. As wind turbines grow in size, the stiffness of the blades and the tower are not increased proportionally, rendering the structure more sensitive to dynamic excitations. Normally, vibrations in the flap-wise direction and tower vibration in the mean wind direction are highly damped due to the strong aerodynamic damping [1]. In contrast, edgewise vibrations and lateral tower vibrations are related with insignificant aerodynamic damping [1,2]. Hence, these modes of vibrations may be prone to large dynamic responses. Most offshore wind turbines are placed at shallow water. Due to refraction, the approaching waves tend to propagate in a direction normal to the level curves of the sea bottom. In turn, this means that the wave load may act in a different direction of the mean wind direction, and significant lateral tower vibrations may be initiated by the wave load in combination with the resultant aerodynamic load from the three blades in the lateral direction.

Some studies have been carried out for the structural control of tower vibrations, most of which focus on passive structural control techniques. Theoretical investigations have been performed on the effectiveness of a tuned mass damper (TMD) [3] and tuned liquid column damper (TLCD) [4] for mitigating along-wind vibrations of wind turbine towers, ignoring the aerodynamic properties of the blades. To yield more realistic results, an advanced modeling tool has been developed and incorporated into the aeroelastic code, FAST (Fatigue, Aerodynamics, Structures and Turbulence), allowing the investigation of passive TMDs in vibration control of offshore wind turbine systems [5]. Recently, a series of shaking table tests have been carried out to evaluate the effect of the ball vibration absorber (BVA) on the vibration mitigation of a reduced scale wind turbine model, which proves the effectiveness of the passive damping device [6]. However, the focus of this study is still on along-wind vibrations without considering the aerodynamic damping. Active structural control of floating wind turbines is investigated by Lackner and Rotea [7]. Simulation results in FAST show that active control is a more effective way of reducing structural loads than the passive control method, at the expense of active power and larger TMD strokes.

For modern variable speed wind turbines, advanced pitch control and generator torque control techniques for the mitigation of structural loads are being increasingly investigated. In a basic variable

speed wind turbine control system, torque control is used in below-rated wind speeds to obtain maximum energy output. Above the rated speed, a pitch controller is utilized to regulate the rotor speed to the desired value, and the generator torque is held constant (nominal torque) [8]. Additional pitch control loops as feedback from measured nacelle fore-aft acceleration are usually used to damp fore-aft tower vibrations [9], although vibration in this direction is already highly damped due to the aerodynamic damping. Generator torque control is widely used to provide damping into the drivetrain torsional vibrations [9–11]. Instead of demanding a constant generator torque above the rated one, an additive torque as feedback from the measured generator speed is added to the torque demand, which is effective at damping vibrations of the resonant mode of the drivetrain.

The idea of providing active damping to lateral tower vibration using generator torque was first proposed by Van der Hooft *et al.* [12] and was further investigated by de Corcuera *et al.* [13] and Fleming *et al.* [14]. Essentially, the generator torque affects the lateral tower vibration through the reaction on the generator stator, which is rigidly fixed to the nacelle. By means of modern power electronics, the generator torque can be prescribed to a certain value with a delay below 10^{-2} s [15]. By using this property, feedback control of the lateral tower vibrations can be performed. Van der Hooft *et al.* [12] simplified the tower by a single-degree-of-freedom (SDOF) representing the lateral translational motion, and the tower top rotation was neglected. Since the generator torque is affecting the lateral tower motion via the tower top rotation, this SDOF tower model does not adequately account for the transfer of the generator torque. De Corcuera *et al.* [13] demonstrated a strategy to design a multi-variable controller based on the H_∞ norm reduction for reducing both the drivetrain torsional vibration and the tower side-to-side vibration, with simulations carried out in the GH Bladed software. This study focuses on the controller design procedure. However, the torque transfer mechanism from the generator to the tower vibration and the effect of the generator torque on other components of the wind turbine are not demonstrated. Fleming *et al.* [14] presented the field-testing results of the effect of active generator control on the drivetrain and lateral tower vibrations in a 600-kW wind turbine. A multi-SISO (single-input-single-output) controller is compared with the H_∞ controller, and a similar effect for damping the lateral tower vibration was obtained. Again, the effect of the generator torque on other components of the wind turbine, such as the blades, was ignored. Actually, the edgewise vibrations of the blades are coupled to the lateral tower vibration, as well as to the torsional drivetrain vibration through the collective mode. Since very low, even negative, aerodynamic damping takes place in edgewise vibration, it is important to investigate the effect of the active generator torque on this mode of vibration. Moreover, as the basis of implementing active generator control, the load transfer mechanisms from the drivetrain and the generator to the nacelle, as well as the interaction between the generator torque with the lateral tower vibration are not clearly demonstrated in the above-mentioned studies. Further, all of the previous studies focus on the gear-driven wind turbines. With offshore wind turbines becoming larger and being moved out further at sea, there is huge application potential of direct-driven systems, where the turbine rotor is coupled directly to the electrical generator without the gearbox. The generators operate at the same rotational speed as the turbine's rotor and must therefore be much bigger in size. However, by using permanent magnets in the generators' rotor and eliminating the gearbox, the weight of the nacelle can be significantly decreased compared to that of the gear-driven system, which, in turn, reduces the shipping and installation costs for offshore wind farms. Further, since the gearbox causes

the greatest downtime resulting in lost revenue, the use of a direct-driven system definitely avoids the cost of overhauling, removing and reinstalling the gearbox, thus reducing operating costs over the long term and making electricity from wind farms more competitive. This is especially important for offshore wind farms, because doing maintenance at sea is a lot more complex and expensive than on the ground. For the direct-driven wind turbines, the electric torque in the generator is much larger comparing with the gear-driven wind turbines, making it possible to damp the lateral tower vibration more effectively.

This paper presents a comprehensive investigation into the modeling and control of lateral tower vibrations in offshore wind turbines using active generator torque, taking into consideration the consequences of the control on the edgewise blade vibrations and the quality of the produced power. The load transfer mechanisms from the generator to the tower are derived in a generalized form for gear-driven wind turbines with an odd or even number of gear stages, as well as for the direct-driven wind turbines. The active generator control algorithm is investigated based on a 13-degrees-of-freedom (13-DOF) wind turbine model developed by the authors, which has been calibrated to the referential 5-MW NREL (National Renewable Energy Laboratory) offshore wind turbine [16]. A three-dimensional (3D) turbulence field is modeled by a low order auto-regressive (AR) model [17]. The dynamic loading from the rotational sampled turbulence and the non-linear aeroelasticity is assumed to be quasi-static, *i.e.*, the changes of aerodynamic forces due to changes of the angle of attack are felt without time delay. The wave load is modeled by the Morison formula [18] in combination with the first order wave theory and applied to the tower in the lateral direction. A generator model is proposed with a complete solution to provide the feedback control torque. Cases of gear-driven and direct-driven wind turbines are both investigated. Simulation results show that lateral tower vibration can be significantly suppressed, and the edgewise vibrations are also slightly mitigated by the active generator control, while only modest influence on the smoothness of the power output are brought about by the additive generator torque.

2. Wind Turbine Model

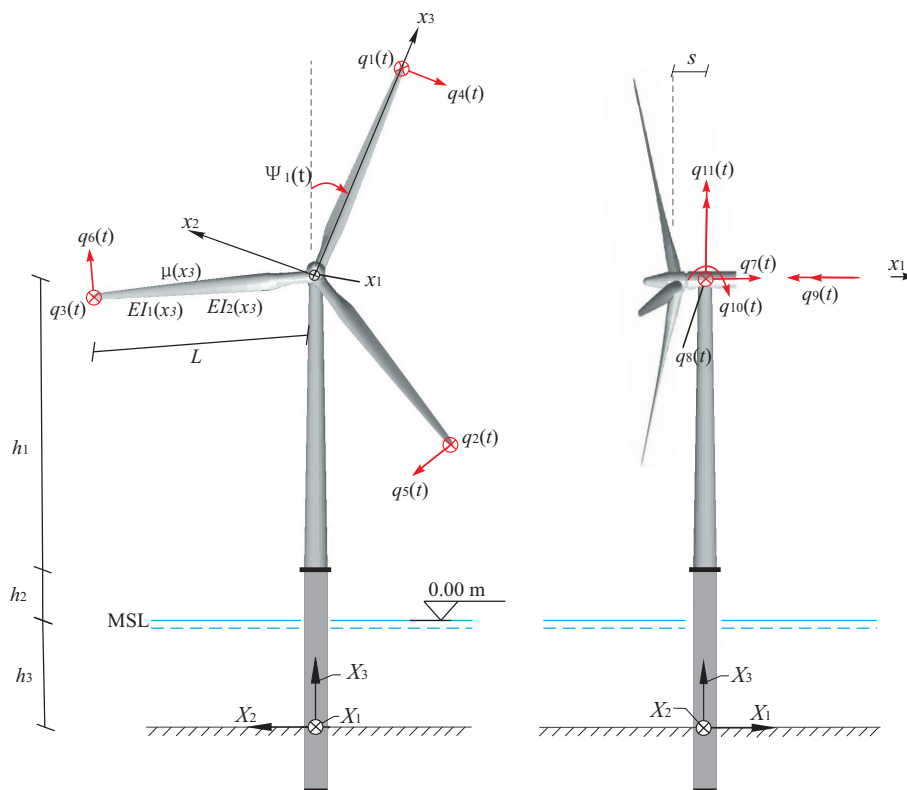
In this section, a 13-DOF aeroelastic wind turbine model is presented with coupled edgewise, lateral tower and torsional drivetrain vibrations. The torque transfer mechanism between the drivetrain and the tower are derived in a generalized manner, which forms the basis for active control of tower vibrations using the generator torque.

2.1. General Description

Despite its simplicity, the 13-DOF aeroelastic model takes into account several important characteristics of a wind turbine, including time-dependent system matrices, coupling of the tower-blades-drivetrain vibration, as well as non-linear aeroelasticity. A schematic representation of the wind turbine model is shown in Figure 1. The motion of structural components is described either in a fixed, global frame of reference (X_1, X_2, X_3) or in moving frames of reference (x_1, x_2, x_3) , attached to each blade with the origin at the center of the hub. Neglecting the tilt of the rotor, the X_1 and x_1 axis are unidirectional to the mean wind velocity. The (X_2, X_3) and (x_2, x_3) coordinate planes are placed in the rotor plane. The X_3 axis is vertical, and the x_3 axis is placed along the blade axis oriented from the hub

towards the blade tip. The position of the moving frame attached to blade j is specified by the azimuthal angle $\Psi_j(t)$, which is considered positive when rotating clockwise seen from an upwind position.

Figure 1. Thirteen DOFs model of a three-bladed wind turbine. Definition of fixed and moving frames of reference and the degrees of freedom $q_1(t), \dots, q_{11}(t)$.

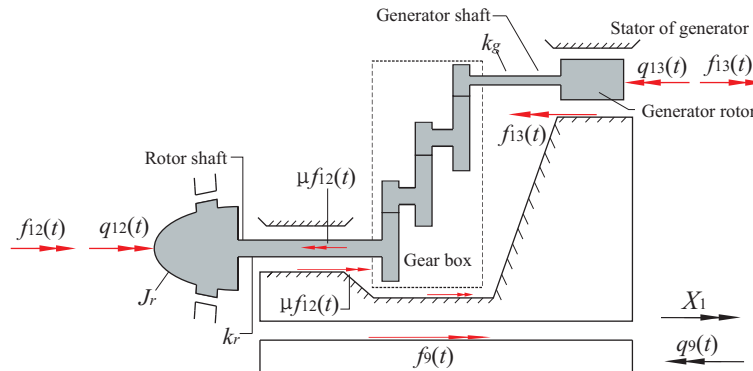


The blades are modeled as Bernoulli–Euler beams with the bending stiffness $EI_1(x_3)$ in the flap-wise direction and $EI_2(x_3)$ in the edgewise direction. The mass per unit length is $\mu(x_3)$. Each blade is related with two degrees of freedom (DOFs). $q_1(t), q_2(t), q_3(t)$ denote the flapwise tip displacement in the positive x_1 direction. $q_4(t), q_5(t), q_6(t)$ denote the edgewise tip displacement in the negative x_2 direction. The length of each blade is denoted L . The tower motion is defined by five DOFs $q_7(t), \dots, q_{11}(t)$. $q_7(t)$ and $q_8(t)$ signify the displacements of the tower at the height of the hub in the global X_1 and X_2 directions. $q_9(t)$ specifies the elastic rotation of the top of the tower in the negative X_1 direction, and $q_{10}(t)$ and $q_{11}(t)$ indicate the corresponding rotations in the positive X_2 and X_3 directions. The height of the tower from the base to the nacelle is denoted h_1 , and the tower base begins at an elevation of h_2 above mean sea level (MSL), with a monopile extending from the tower base to the mud line. The water depth from the mud line to the MSL is denoted h_3 , and the horizontal distance from the center of the tower top to the origin of the moving coordinate systems is denoted s (Figure 1).

The drivetrain is modeled by the DOFs $q_{12}(t)$ and $q_{13}(t)$ (Figure 2). The sign definition shown in Figure 2 applies to a gearbox with an odd number of stages. $q_{12}(t)$ and $q_{13}(t)$ indicate the deviations of the rotational angles at the hub and the generator from the nominal rotational angles Ωt and $N\Omega t$, respectively, where N is the gear ratio. Correspondingly, $\dot{q}_{12}(t)$ and $\dot{q}_{13}(t)$ are the deviations of the rotational speeds at the hub and the generator from the nominal values. In case of an even number of stages, the sign definitions for $q_{13}(t)$ and $f_{13}(t)$ are considered positive in the opposite direction. J_r and

J_g denote the mass moment of inertia of the rotor and the generator; and k_r and k_g denote the St. Venant torsional stiffness of the rotor shaft and the generator shaft. The azimuthal angle of the blade j (Figure 1) becomes $\Psi_j(t) = \Omega t + q_{12}(t) + \frac{2\pi}{3}(j - 1)$, $j = 1, 2, 3$.

Figure 2. Two DOFs model of flexible drivetrain with an odd number of gear stages. Definition of degrees of freedom $q_{12}(t)$ and $q_{13}(t)$.



Further, a full-span rotor-collective pitch controller is included in the model with time delay modeled by a first order filter. The pitch demand is modeled by a PI controller [19] with feedback from $\dot{q}_{12}(t)$ and $q_{12}(t)$. A gain-scheduled PI controller is used in this paper, *i.e.*, the controller gains are dependent on the blade-pitch angle [16].

2.2. Coupled Edgewise, Lateral Tower and Torsional Drivetrain Vibrations

The equations of motion of the 13-DOF wind turbine model can be derived from the Euler–Lagrange equation [20]:

$$\frac{d}{dt} \left(\frac{\partial T}{\partial \dot{\mathbf{q}}} \right) - \frac{\partial T}{\partial \mathbf{q}} + \frac{\partial U}{\partial \mathbf{q}} = \mathbf{f}(t) \tag{1}$$

where $\mathbf{q}^T(t) = [q_1(t), \dots, q_{13}(t)]$ is a 13-dimensional column vector storing all DOFs. $T = T(\mathbf{q}, \dot{\mathbf{q}})$ signifies the kinetic energy, and $U = U(\mathbf{q})$ is the potential energy of the system. The key step in setting up the coupled equation is to formulate the kinetic energy of each blade with velocity contributions from both the locally and globally defined DOFs. For example, $\dot{q}_1(t), \dot{q}_7(t), \dot{q}_{10}(t)$ and $\dot{q}_{11}(t)$ induce the velocity component of a cross-section of Blade 1 in the x_1 direction, while $\dot{q}_4(t), \dot{q}_8(t), \dot{q}_{10}(t), \dot{q}_{11}(t)$ and $\dot{q}_{12}(t)$ induce the velocity component of Blade 1 in the x_2 direction. $\mathbf{f}(t)$ is the force vector work conjugated to $\mathbf{q}(t)$, including structural damping forces, aerodynamic and hydrodynamic forces, as well as generator control forces.

Assuming linear structural dynamics and substituting the expressions for kinetic and potential energies into Equation (1), the equations of motion of the 13-DOF wind turbine model are obtained of the form:

$$\mathbf{M}(t) \ddot{\mathbf{q}}(t) + \mathbf{C}(t) \dot{\mathbf{q}}(t) + \mathbf{K}(t) \mathbf{q}(t) = \mathbf{f}_e(t) \tag{2}$$

where $\mathbf{M}(t)$ is the mass matrix, $\mathbf{C}(t)$ is the damping matrix, including the structural damping and the gyroscopic damping, and $\mathbf{K}(t)$ is the stiffness matrix taking into account the geometric stiffness

and the gyroscopic stiffness. Both the gyroscopic damping matrix and gyroscopic stiffness matrix are obtained by substituting the kinetic energy of the system into the Euler–Lagrange equation. Through this procedure, the coriolis forces and the centrifugal softening effect are taken into account. $\mathbf{f}_e(t)$ is the external dynamic load vector work conjugated to $\mathbf{q}(t)$, which is composed of the non-linear aerodynamic loads, the generator torque and the wave loads. All of the indicated system matrices are time dependent, due to the fact that the DOFs of the blades are formulated in the moving frames of reference, and others are formulated in a fixed frame of reference.

Next, the DOFs vector $\mathbf{q}(t)$ may be partitioned in the following way:

$$\mathbf{q}(t) = \begin{bmatrix} \mathbf{q}_1(t) \\ \mathbf{q}_2(t) \end{bmatrix} \tag{3}$$

$$\begin{aligned} \mathbf{q}_1^T(t) &= [q_4(t) \quad q_5(t) \quad q_6(t) \quad q_8(t) \quad q_9(t) \quad q_{12}(t) \quad q_{13}(t)] \\ \mathbf{q}_2^T(t) &= [q_1(t) \quad q_2(t) \quad q_3(t) \quad q_7(t) \quad q_{10}(t) \quad q_{11}(t)] \end{aligned} \tag{4}$$

The main focus of the present study is on the dynamic coupling of edgewise, lateral tower and torsional drivetrain motions and the effect of active generator torque on these vibrations. To clearly unfold this coupling, only the sub-system related to DOFs $\mathbf{q}_1(t)$ is picked out from Equation (2) and is demonstrated in detail. It should be noted that the numerical simulations in the subsequent section will always be based on Equation (2), where all of the 13 DOFs are activated. As a part of Equation (2), the equations of motion related to the above-mentioned sub-system, which show the coupling of edgewise, lateral tower and torsional drivetrain vibrations, are demonstrated by the following matrix differential equations:

$$\mathbf{M}_1(t) \ddot{\mathbf{q}}_1(t) + \mathbf{C}_1(t) \dot{\mathbf{q}}_1(t) + \mathbf{K}_1(t) \mathbf{q}_1(t) = \mathbf{f}_{e,1}(t) \tag{5}$$

$$\mathbf{M}_1(t) = \begin{bmatrix} m_2 & 0 & 0 & -m_1 \cos \Psi_1 & 0 & m_3 & 0 \\ 0 & m_2 & 0 & -m_1 \cos \Psi_2 & 0 & m_3 & 0 \\ 0 & 0 & m_2 & -m_1 \cos \Psi_3 & 0 & m_3 & 0 \\ -m_1 \cos \Psi_1 & -m_1 \cos \Psi_2 & -m_1 \cos \Psi_3 & m_{88} + M_0 + 3m_0 & m_{89} & 0 & 0 \\ 0 & 0 & 0 & m_{98} & m_{99} & 0 & 0 \\ m_3 & m_3 & m_3 & 0 & 0 & J_r & 0 \\ 0 & 0 & 0 & 0 & 0 & 0 & J_g \end{bmatrix}$$

$$\mathbf{C}_1(t) = \begin{bmatrix} c_2 & 0 & 0 & 0 & 0 & 0 & 0 \\ 0 & c_2 & 0 & 0 & 0 & 0 & 0 \\ 0 & 0 & c_2 & 0 & 0 & 0 & 0 \\ 2\Omega m_1 \sin \Psi_1 & 2\Omega m_1 \sin \Psi_2 & 2\Omega m_1 \sin \Psi_3 & c_{88} & c_{89} & 0 & 0 \\ 0 & 0 & 0 & c_{98} & c_{99} & 0 & 0 \\ 0 & 0 & 0 & 0 & 0 & 0 & 0 \\ 0 & 0 & 0 & 0 & 0 & 0 & 0 \end{bmatrix}$$

$$\mathbf{K}_1(t) = \begin{bmatrix} k_2 - k_g & 0 & 0 & 0 & 0 & 0 & 0 & 0 \\ 0 & k_2 - k_g & 0 & 0 & 0 & 0 & 0 & 0 \\ 0 & 0 & k_2 - k_g & 0 & 0 & 0 & 0 & 0 \\ \Omega^2 m_1 \cos \Psi_1 & \Omega^2 m_1 \cos \Psi_2 & \Omega^2 m_1 \cos \Psi_3 & k_{88} & k_{89} & 0 & 0 & 0 \\ 0 & 0 & 0 & k_{98} & k_{99} & 0 & 0 & 0 \\ 0 & 0 & 0 & 0 & 0 & k_0 & -\frac{k_0}{N} & 0 \\ 0 & 0 & 0 & 0 & 0 & -\frac{k_0}{N} & \frac{k_0}{N^2} & 0 \end{bmatrix} \quad (6)$$

where:

$$m_0 = \int_0^L \mu(x_3) dx_3, m_1 = \int_0^L \Phi(x_3) \mu(x_3) dx_3, m_2 = \int_0^L \Phi^2(x_3) \mu(x_3) dx_3, m_3 = \int_0^L \Phi(x_3) \mu(x_3) x_3 dx_3 \quad (7)$$

$$k_2 = \int_0^L \left(EI_2(x_3) \left(\frac{d^2 \Phi(x_3)}{dx_3^2} \right)^2 + F(x_3) \left(\frac{d\Phi(x_3)}{dx_3} \right)^2 \right) dx_3, \quad k_g = \Omega^2 m_2, \quad J_r = 3 \int_0^L \mu(x_3) x_3^2 dx_3$$

$\Phi(x_3)$ is the undamped eigenmode in the edgewise direction, when the blade is fixed at the hub. Due to the definition of $q_{j+3}(t)$, $j = 1, 2, 3$, this mode must be normalized to one at the tip, i.e., $\Phi(L) = 1$. $F(x_3) = \Omega^2 \int_{x_3}^L \mu(\xi) \xi d\xi$ is the centrifugal axial force on the blade. m_0 is the mass of each blade, and M_0 is the mass of the nacelle. $c_2 = 2\zeta_2 \sqrt{m_2 k_2}$ is the modal damping coefficient of the edgewise vibration, calculated from the given damping ratio ζ_2 .

As shown in Figure 3, the lateral tower vibration is modeled by two DOFs, $q_8(t)$ and $q_9(t)$, with cubic shape functions $N_8(X_3)$ and $N_9(X_3)$, respectively. The consistent mass and stiffness terms for $q_8(t)$ and $q_9(t)$ are calculated from the tower itself without considering the nacelle and the rotor, as given by the following equation:

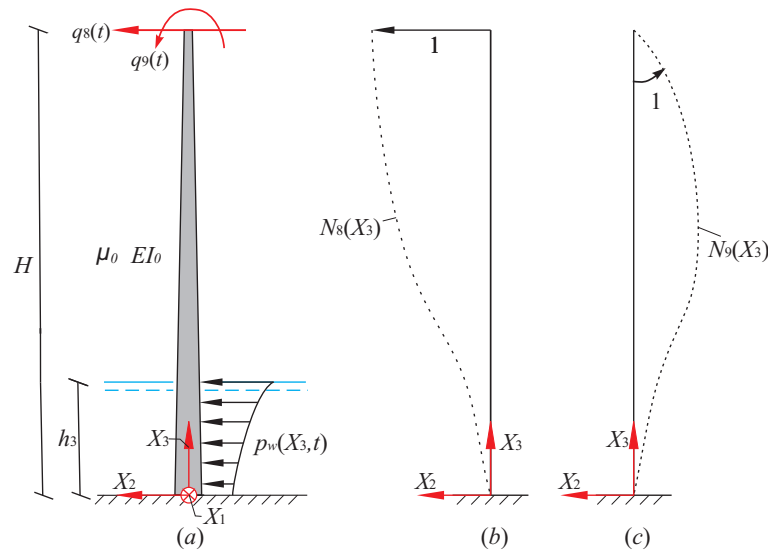
$$m_{88} = \int_0^H \mu_0(X_3) N_8^2(X_3) dX_3, \quad m_{89} = \int_0^H \mu_0(X_3) N_8(X_3) N_9(X_3) dX_3, \quad m_{99} = \int_0^H \mu_0(X_3) N_9^2(X_3) dX_3 \quad (8)$$

$$k_{88} = \int_0^H EI_0(X_3) \left(\frac{\partial N_8}{\partial X_3} \right)^2 dX_3, \quad k_{89} = \int_0^H EI_0(X_3) \left(\frac{\partial N_8}{\partial X_3} \right) \left(\frac{\partial N_9}{\partial X_3} \right) dX_3, \quad k_{99} = \int_0^H EI_0(X_3) \left(\frac{\partial N_9}{\partial X_3} \right)^2 dX_3$$

where $\mu_0(X_3)$ and $EI_0(X_3)$ are the mass per unit length and bending stiffness in the lateral direction of the tower, respectively. $N_8(X_3) = 3 \left(\frac{X_3}{H} \right)^2 - 2 \left(\frac{X_3}{H} \right)^3$, $N_9(X_3) = H \left(\left(\frac{X_3}{H} \right)^3 - \left(\frac{X_3}{H} \right)^2 \right)$, $H = h_1 + h_2 + h_3$ is the total height of the tower structure. The related damping terms c_{88} , c_{89} , c_{98} , c_{99} are specified by the Rayleigh damping model [21] from the consistent mass and stiffness terms, with given damping ratios ζ_8 and ζ_9 . k_0 indicates an equivalent torsional stiffness of the shaft of the drivetrain, given as:

$$\frac{1}{k_0} = \frac{1}{k_r} + \frac{1}{N^2 k_g} \quad \Rightarrow \quad k_0 = \frac{N^2 k_r k_g}{k_r + N^2 k_g} \quad (9)$$

Figure 3. Modeling of the lateral tower vibration. (a) Two DOFs model for lateral tower vibration with wave loads. (b) Shape function for the degree of freedom $q_8(t)$. (c) Shape function for the degree of freedom $q_9(t)$.



From Equation (6), it is noted that the edgewise vibrations are coupled to the lateral tower vibration through the mass matrix, damping matrix and stiffness matrix and coupled to the drivetrain torsional vibration through the mass matrix alone. Actually, only the collective mode of the edgewise vibration is coupled with the torsional vibration of the drivetrain.

2.3. Torque Transfer Mechanism between the Drivetrain and the Tower

In Equation (5), the external dynamic load vector work conjugated to $\mathbf{q}_1(t)$ is expressed as:

$$\mathbf{f}_{e,1}^T(t) = \left[f_4(t) \quad f_5(t) \quad f_6(t) \quad f_8(t) \quad f_9(t) \quad (1 - \mu)f_{12}(t) \quad -f_{13}(t) \right] \quad (10)$$

where $f_4(t)$, $f_5(t)$, $f_6(t)$ and $f_{12}(t)$ are dynamic loads work-conjugated to the defined DOFs, resulting from aerodynamic loads. $f_8(t)$ is the load work-conjugated to the degree of freedom $q_8(t)$, due to both aerodynamic loads and wave forces. $(1 - \mu)f_{12}(t)$ denotes the effective torque on the drivetrain available for power production due to friction in the bearings and the gear box, as specified by the friction coefficient μ . $f_{13}(t)$ indicates the generator torque.

Using D'Alembert's principle, the net torque on the drivetrain in the global X_1 direction becomes $(1 - \mu)f_{12}(t) - J_r\ddot{q}_{12}(t) \pm (f_{13}(t) + J_g\ddot{q}_{13}(t))$, where the plus sign applies for a gearbox with an odd number of gear stages (as shown in Figure 2) and the minus sign for an even number of stages. The torque is transferred to the nacelle in the positive X_1 direction via the bearings of the shaft and the gearbox. On the nacelle, the transferred torque is added to the reaction of the friction torque $\mu f_{12}(t)$ (always in the positive X_1 direction) and the generator torque on the stator $f_{13}(t)$, which is acting in the negative X_1 direction for an odd number of stages or acting in the positive X_1 direction for an even number of stages. Hence, the resultant torque on the bottom of the nacelle becomes $f_{12}(t) - J_r\ddot{q}_{12}(t) \pm J_g\ddot{q}_{13}(t)$ (plus sign for an odd number of gear stages). With $q_9(t)$ defined as positive when acting in the negative X_1 direction, the torque work-conjugated to $q_9(t)$ resulting from the nacelle becomes $-f_{12}(t) + J_r\ddot{q}_{12}(t) \mp J_g\ddot{q}_{13}(t)$

(minus sign for an odd number of gear stages). Then, together with the contribution from the wave load, the total load work-conjugated to $q_9(t)$ becomes:

$$f_9(t) = \begin{cases} f_{9,w}(t) - f_{12}(t) + J_r \ddot{q}_{12}(t) - J_g \ddot{q}_{13}(t) & \text{(odd number of gear stages)} \\ f_{9,w}(t) - f_{12}(t) + J_r \ddot{q}_{12}(t) + J_g \ddot{q}_{13}(t) & \text{(even number of gear stages)} \end{cases} \quad (11)$$

where $f_{9,w}(t)$ is the load conjugated to $q_9(t)$ induced by waves propagating in the X_2 direction. As shown in Figure 3, $p_w(X_3, t)$ denotes the distributed wave force acting on the tower, which can be calculated by the Morison formula. Then, the loads conjugated to $q_8(t)$ and $q_9(t)$ induced by the distributed wave force can be written as:

$$\begin{bmatrix} f_{8,w}(t) \\ f_{9,w}(t) \end{bmatrix} = \int_0^{h_3} \begin{bmatrix} N_8(X_3) \\ N_9(X_3) \end{bmatrix} p_w(X_3, t) dX_3 \quad (12)$$

The control of the lateral tower vibration is actually applied via the torque $f_9(t)$ conjugated to $q_9(t)$. For this reason, the relation between $f_9(t)$ and $f_{13}(t)$ is analyzed. The equation of motion of the drivetrain reads from Equations (5) and (10):

$$\begin{bmatrix} J_r & 0 \\ 0 & J_g \end{bmatrix} \begin{bmatrix} \ddot{q}_{12}(t) \\ \ddot{q}_{13}(t) \end{bmatrix} + k_0 \begin{bmatrix} 1 & -\frac{1}{N} \\ -\frac{1}{N} & \frac{1}{N^2} \end{bmatrix} \begin{bmatrix} q_{12}(t) \\ q_{13}(t) \end{bmatrix} = \begin{bmatrix} (1 - \mu)f_{12}(t) \\ -f_{13}(t) \end{bmatrix} \quad (13)$$

The acceleration terms in Equation (11) can be eliminated by means of the equation of motion of the drivetrain, resulting in the equivalent expression for $f_9(t)$:

$$f_9(t) = \begin{cases} f_{9,w}(t) - \mu f_{12}(t) + f_{13}(t) - k_0 \left(1 + \frac{1}{N}\right) \left(q_{12}(t) - \frac{1}{N} q_{13}(t)\right) & \text{(odd number of gear stages)} \\ f_{9,w}(t) - \mu f_{12}(t) - f_{13}(t) - k_0 \left(1 - \frac{1}{N}\right) \left(q_{12}(t) - \frac{1}{N} q_{13}(t)\right) & \text{(even number of gear stages)} \end{cases} \quad (14)$$

Especially for direct-driven wind turbines, where $N = 1$, we get from the second equation in Equation (14) that:

$$f_9(t) = f_{9,w}(t) - \mu f_{12}(t) - f_{13}(t) \quad (15)$$

It is seen from the last part of the two sub-equations in Equation (14) that for gear-driven wind turbines, there are extra coupling terms between the degree of freedom $q_9(t)$ and the two DOFs of the drivetrain, which can be transferred and added to the stiffness matrix in Equation (6). Based on the relationship between $f_9(t)$ and $f_{13}(t)$ in Equations (14) and (15), the lateral tower vibrations can be controlled by specifying the format of the generator torque $f_{13}(t)$, as will be shown in the subsequent section.

2.4. Aerodynamic and Wave Loads

In agreement with [22], the turbulence modeling is based on Taylor’s hypothesis of frozen turbulence, corresponding to a frozen turbulence field that is convected into the rotor in the global X_1 direction with a mean velocity V_0 , which provides the relation between spatial coordinates and time. The frozen field is assumed to be a zero mean homogeneous and isotropic stochastic field, with a spatial covariance structure given by [23]. Calibrated from the theoretical covariance structure, the first order AR model as proposed by [17] performs a first-order filtering of the white noise input, resulting in continuous, non-differentiable

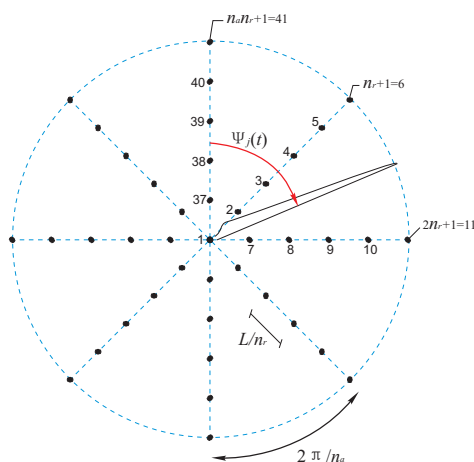
sample curves of the turbulence field at the rotor plane in the fixed frame of reference. As shown in Figure 4, the fixed frame components of the convected turbulence are generated at $n_n = n_a \cdot n_r + 1$ nodal points at the discrete instants of time $t = 0, \Delta t, 2\Delta t, \dots$, where n_a is the number of radial lines in the mesh from the center Node 1 and n_r is the number of equidistantly placed nodes along a given radial line. Next, the fixed frame components of the rotational sampled turbulence vector on each blade with the azimuthal angle Ψ_j are obtained by linear interpolation of the turbulence of the adjacent radial lines according to the position of the blade at each time step. Finally, the moving frame components of the rotational sampled turbulence are obtained by the following coordinate transformation:

$$\begin{bmatrix} v_{1,j}(x_3, t) \\ v_{2,j}(x_3, t) \\ v_{3,j}(x_3, t) \end{bmatrix} = \begin{bmatrix} 1 & 0 & 0 \\ 0 & \cos \Psi_j & \sin \Psi_j \\ 0 & -\sin \Psi_j & \cos \Psi_j \end{bmatrix} \begin{bmatrix} \bar{v}_{1,j}(\mathbf{X}, t) \\ \bar{v}_{2,j}(\mathbf{X}, t) \\ \bar{v}_{3,j}(\mathbf{X}, t) \end{bmatrix} \tag{16}$$

where $v_{1,j}(x_3, t)$, $v_{2,j}(x_3, t)$ and $v_{3,j}(x_3, t)$ are rotational sampled turbulence components for blade j at the position x_3 , in the moving frames of reference. $\bar{v}_{1,j}(\mathbf{X}, t)$, $\bar{v}_{2,j}(\mathbf{X}, t)$, $\bar{v}_{3,j}(\mathbf{X}, t)$ are rotational sampled turbulence components at the same position for blade j in the fixed frame of reference with $\mathbf{X} = [0, -x_3 \sin \Psi_j, x_3 \cos \Psi_j]^T$. Due to the longitudinal correlation of the incoming turbulence, a certain periodicity is present as spectral peaks at $1\Omega, 2\Omega, 3\Omega\dots$ in the frequency domain representation of the rotational sampled turbulence. The simple AR model used here does not represent the low-frequency, large-scale turbulent structures very well, due to the homogeneity and isotropy assumption. On the other hand, the dynamics of the tower are more related to the frequency component of turbulence in the vicinity of the tower frequency. In this respect, the rotational sampled effect seems to be more important and is well accounted for by the present model.

The blade element momentum (BEM) method with Prandtl’s tip loss factor and Glauert correction is adopted to calculate aerodynamic forces along the blade [24]. Non-linear aeroelasticity is considered by including the local deformation velocities of the blade into the calculation of the flow angle and the angle of attack. As a result, high aerodynamic damping is introduced in the blade flap-wise and the fore-aft tower vibrations, but relatively low aerodynamic damping in the blade edgewise and the lateral tower vibrations.

Figure 4. Nodal points in the rotor plane of the discretized turbulence field. $n_a = 8, n_r = 5$.



Sea surface elevation is modeled as a zero mean, stationary Gaussian process defined by the single-sided version of the JONSWAP (Joint North Sea Wave Project) spectrum [25], which is determined by the significant wave height H_s and the peak period T_p . Assuming first order wave theory, the realization of the stationary wave surface elevation process can be obtained by the following random phase model:

$$\eta(X_2, t) = \sum_{j=1}^J \sqrt{2}\eta_j \cos(\omega_j t - k_j X_2 + \phi_j) \quad (17)$$

where J is the number of harmonic components in the spectral decomposition, ω_j and k_j are the angular frequency and wave number of the j -th harmonic component related through the dispersion relationship $\omega_j^2 = gk_j \tanh(k_j h)$. ϕ_j denotes samples of the random phase Φ_j , which are mutually independent and uniformly distributed in $[0, 2\pi]$. $\eta_j = \sqrt{S_\eta(\omega_j)\Delta\omega_j}$ denotes the standard deviation of the j -th harmonic component, and $S_\eta(\omega_j)$ is the single-sided JONSWAP spectrum.

Following the linear wave theory, the horizontal velocity $v(X_3, t)$ and acceleration $\dot{v}(X_3, t)$ of the water particle at the position $X_2 = 0$ can be written as:

$$\begin{aligned} v(X_3, t) &= \sum_{j=1}^J \sqrt{2}\eta_j \omega_j \frac{\cosh(k_j X_3)}{\sinh(k_j h)} \cos(\omega_j t + \phi_j) \\ \dot{v}(X_3, t) &= - \sum_{j=1}^J \sqrt{2}\eta_j \omega_j^2 \frac{\cosh(k_j X_3)}{\sinh(k_j h)} \sin(\omega_j t + \phi_j) \end{aligned} \quad (18)$$

The distributed wave force acting at the position X_3 of the tower can be calculated by the Morison Equation [18]:

$$p_w(X_3, t) = \frac{1}{2}\rho_w C_d D v(X_3, t) |v(X_3, t)| + \frac{\pi}{4}\rho_w C_m D^2 \dot{v}(X_3, t) \quad (19)$$

where ρ_w is the fluid density, C_d is the drag coefficient, C_m is the inertia coefficient and D is the diameter of the turbine monopile. The total wave forces can then be calculated by Equation (12), which are acting on the wind turbine tower perpendicularly to the mean wind direction.

3. Active Generator Control

A simple active control algorithm is proposed based on active generator torque with feedback from the measured lateral tower vibrations. Closed-loop equations are obtained from the active control. A full-scale power converter configuration with a cascaded loop control structure is also introduced to produce the feedback torque in real time.

3.1. Closed-Loop Equations from Active Control

Only the above rated region (Region 3 according to [16]) is considered where the mean wind speed is higher than the rated value, and the wind turbine produces nominal power with the functioning of the collective pitch controller. In the basic control system for Region 3, the collective pitch controller is activated to regulate the rotor speed to the nominal value, while the generator torque is held constant [9]. Modern power electronics makes it possible to specify the generator torque within certain limits almost instantly (time delay below 10^{-2} s). Then, the generator torque $f_{13}(t)$ can be used as an actuator in the

active vibration control of the structure. Sometimes, a torsional damping term as feedback control is included in the generator torque to damp the resonant mode of the drivetrain [10]. Since the focus is to investigate the effectiveness of active generator control of lateral tower vibrations and the influence of the controller on the power output, as well as on the responses of other components, the torsional damping term is not taken into account in the present study. The generator controller with feedback from lateral tower vibrations is proposed as:

$$f_{13}(t) = f_{13,0} + \Delta f_{13,0}(t) = f_{13,0} + c_a \dot{q}_8(t) \tag{20}$$

where $f_{13,0} = \frac{P_0}{N\Omega}$ is the constant nominal torque and P_0 is the nominal power produced by the wind turbine. With the functioning of the collective pitch controller, $f_{13,0}$ is balanced by the mean value of the aerodynamic torque on the rotor. $c_a \dot{q}_8(t)$ is the feedback torque components from lateral tower velocity, and c_a is the gain factor. In practical applications, the feedback signal $\dot{q}_8(t)$ is obtained by integrating the measured tower top acceleration from accelerometers placed in the nacelle.

Then, the generated power becomes:

$$P(t) = \left(f_{13,0} + \Delta f_{13,0}(t) \right) \left(N\Omega + \dot{q}_{13}(t) \right) = P_0(t) + \Delta P(t) \tag{21}$$

where $P_0 = N\Omega f_{13,0}$ is the nominal power of the wind turbine, and $\Delta P(t) = \Delta f_{13,0}(t) (N\Omega + \dot{q}_{13}(t)) + f_{13,0} \dot{q}_{13}(t)$ indicates a time-varying deviation from the nominal power. In the absence of the active generator control, *i.e.*, $c_a = 0$, the deviation of power output only contains the term $f_{13,0} \dot{q}_{13}(t)$. With active generator control, fluctuation of the power output is introduced by the term $\Delta f_{13,0}(t) (N\Omega + \dot{q}_{13}(t))$ due to the torque increment $\Delta f_{13,0}(t)$. From a power electronic point of view, it is favorable that $\Delta P(t)$ is as small as possible in comparison with P_0 in order to have a smooth power output. From a vibration point of view, it is favorable to have larger c_a and, hence, $\Delta P(t)$, introducing higher damping to the lateral tower mode. Consequently, there is a tradeoff between these two objectives. In this respect, the gain factors c_a is chosen such that the following performance criterion is minimized:

$$J(c_a) = W \frac{\sigma_{q_8}}{\sigma_{q_8,0}} + (1 - W) \frac{\sigma_P}{\sigma_{P,0}}, \quad 0 < W < 1 \tag{22}$$

where $\sigma_{q_8,0}$ and $\sigma_{P,0}$ signify the standard deviation of the lateral tower top displacement $q_8(t)$ and the power output without active generator control, *i.e.*, the generator torque is kept constant as $f_{13,0}$. σ_{q_8} and σ_P denote the standard deviation of $q_8(t)$ and the power output, when active generator control is implemented using Equation (20), and W is the weighting factor for the lateral tower vibration. It is clear that by increasing the value of W , more importance is placed on maintaining small values for the lateral tower vibration.

The torque $f_9(t)$ work-conjugated to $q_9(t)$ for wind turbines with an active generator controller follows from Equations (14) and (20):

$$f_9(t) = \begin{cases} f_{9,w}(t) - \mu f_{12}(t) + f_{13,0} + c_a \dot{q}_8(t) - k_0 \left(1 + \frac{1}{N} \right) \left(q_{12}(t) - \frac{1}{N} q_{13}(t) \right) & \text{(odd stages)} \\ f_{9,w}(t) - \mu f_{12}(t) - f_{13,0} - c_a \dot{q}_8(t) - k_0 \left(1 - \frac{1}{N} \right) \left(q_{12}(t) - \frac{1}{N} q_{13}(t) \right) & \text{(even stages)} \end{cases} \tag{23}$$

Substituting Equations (20) and (23) into the load vector (Equation (10)) at the right-hand side of Equation (5), the equation of motion of the system with active generator controller is given by:

$$M_1(t) \ddot{q}_1(t) + (C_1(t) + C_a(t)) \dot{q}_1(t) + K_1(t) q_1(t) = f_{e,1}(t) \tag{24}$$

where:

$$C_a(t) = \begin{bmatrix} 0 & 0 & 0 & 0 & 0 & 0 & 0 \\ 0 & 0 & 0 & 0 & 0 & 0 & 0 \\ 0 & 0 & 0 & 0 & 0 & 0 & 0 \\ 0 & 0 & 0 & 0 & 0 & 0 & 0 \\ 0 & 0 & 0 & \mp c_a & 0 & 0 & 0 \\ 0 & 0 & 0 & 0 & 0 & 0 & 0 \\ 0 & 0 & 0 & c_a & 0 & 0 & 0 \end{bmatrix} \tag{25}$$

The system matrices $M_1(t)$, $C_1(t)$, $K_1(t)$ and the load vector $f_{e,1}(t)$ are unchanged, except that an extra damping matrix $C_a(t)$ is introduced by the active generator controller. Therefore by making use of the extra damping matrix, it is possible to mitigate lateral tower vibrations, as will be shown in the following simulation results. The upper sign in Equation (25) refers to the gearbox with an odd number of stages, while the lower sign corresponds to the case with an even number of gear stages, which also applies to the direct-driven wind turbines (the number of stages is zero).

3.2. Power Electronic Solution for Torque Control

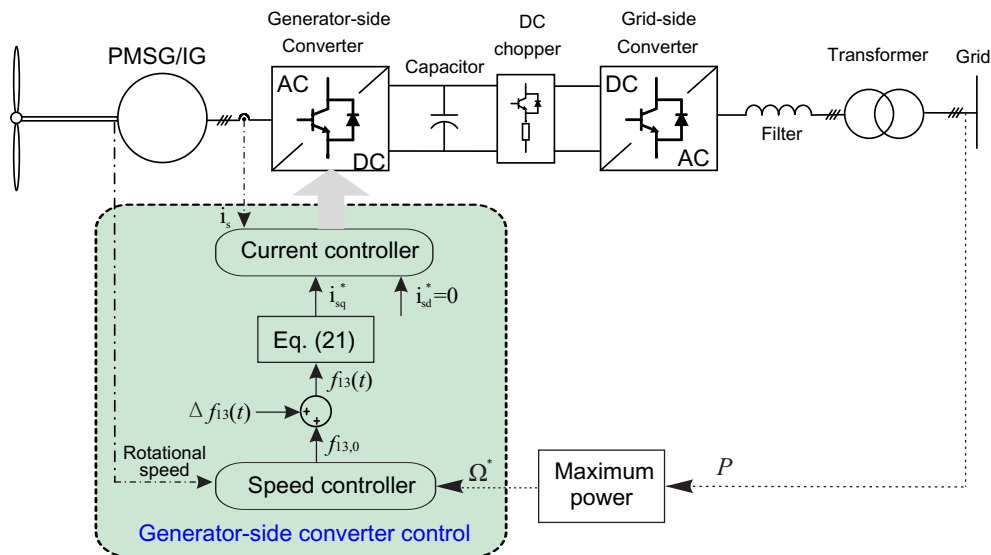
In order to realize the objective of active control of lateral tower vibration using the generator torque, a generator model is introduced. As seen in Figure 5, a full-scale power converter configuration equipped with a permanent magnet synchronous generator (PMSG) or an induction generator (IG) is considered [15]. Normally, a PMSG-based wind turbine may become a direct-driven system, which avoids the fatigue-prone gearbox. The principle of the full-scale power converter is the same for both IG and PMSG. The generator stator winding is connected to the grid through a full-scale back-to-back power converter, which performs the reactive power compensation and a smooth grid connection. Due to different positions, the back-to-back power converter is named as the generator-side converter and the grid-side converter, respectively. The grid-side converter is used to keep the DC-link voltage V_{DC} fixed and to meet the reactive power demand according to the grid codes [26].

The active generator control scheme for lateral tower vibration is carried out via the generator-side converter. With the aid of the stator field oriented control (as shown in Figure 5), a cascaded loop control structure is realized by two controllers: outer speed loop and inner current loop. According to the maximum power tracking point, the rotor speed demand is calculated by the measured power fed into grid. Above the rated region, the speed control loop provides a torque demand of $f_{13,0}$. Along with additive generator torque demand $c_a \dot{q}_8(t)$, the total torque demand is given in the same form as Equation (20). The electromagnetic torque T_e of the generator can be expressed as [27]:

$$T_e = \frac{3}{2} p \Psi_m i_{sq} \tag{26}$$

where p denotes the number of pole pairs, Ψ_m denotes the flux induced by the magnet and i_{sq} denotes the stator current in the q axis. It is noted that the electromagnetic torque is only in line with the q axis stator current. As a consequence, the electromagnetic torque can be simply controlled by the inner current loop together with the demand of the d axis current setting at zero for minimum power loss.

Figure 5. Control diagram in a wind turbine with a permanent magnet synchronous generator or an induction generator.



From the power electronic point of view, direct driven and gear-driven wind turbines are basically dependent on which kind of generator the manufacturer prefers to use. If the synchronous generator is selected, due to the relatively low speed of the generator rotor, the wind turbine system could have less stages of the gearbox or even becomes direct-driven if the poles of the generator are high enough (e.g., permanent-magnet synchronous generator). On the other hand, if the induction generator is chosen, the gearbox must be employed because of its high rotor speed range, which cannot match the speed of the wind turbine rotor directly.

4. Results and Discussion

Numerical simulations are carried out on the calibrated 13-DOF model subjected to the wave and wind loads. In all simulations, the same turbulent wind field and wave loads have been used, with the mean wind velocity $V_0 = 15$ m/s, the turbulence intensity $I = 10\%$, the significant wave height $H_s = 2$ m and the time interval $\Delta t = 0.02$ s. The worst case study scenario is considered, *i.e.*, the wave loads are acting on the tower in the lateral direction perpendicular to the mean wind velocity. Both gear-driven and direct-driven wind turbines are investigated to evaluate the effectiveness of active generator torque on mitigating lateral tower vibrations.

4.1. Model Calibration

The NREL 5-MW referential wind turbine [16] together with the monopile-type support structure documented by [28] are used to calibrate the proposed 13-DOF aeroelastic model. The rotor-nacelle

assembly of the NREL 5-MW wind turbine, including the aerodynamic, structural and pitch control system properties, remains the same as in [16]. This wind turbine is mounted atop a monopile foundation at a 20-m water depth, and the tower base begins at an elevation of 10 m above mean sea level (MSL). As for the rotor, each blade has eight different airfoil profiles from hub to tip, the lift and drag coefficients of which are obtained by wind tunnel tests. The related data of the modal shapes, the bending stiffness and the mass per unit length of the blade are also given by [16]. As for the support-structure, the distributed properties of the tower and monopile are given by [28]. Based on these data, we can calculate the parameters of the rotor and the support structure (the geometries, the mass parameters and the stiffness parameters) in the 13-DOF model, as presented in Table 1. Next, to evaluate the validity and feasibility of the proposed 13-DOF model, comparisons of some results obtained from the present model and from the NREL FAST program [16] are carried out. Table 2 shows the results for the natural frequencies of the blade and the tower, as well as the steady-state responses of the blade, the tower and the pitch controller at different mean wind speeds. The steady-state responses of the present model are obtained by running simulations on the 13-DOF system at three given, steady and uniform wind speeds, when the turbulence field is inactivated. The simulation lengths are long enough to ensure that all transient behavior has died out. The FAST results for the blade and the pitch controller are given by [16], and the results for the tower are given by [28]. The agreement between FAST and the 13-DOF model is quite good, which validates the present model.

Table 1. Parameters in the 13-DOF wind turbine model.

Parameter	Value	Unit	Parameter	Vale	Unit
L	61.50	m	k_2	5.80×10^4	N/m
h_1	77.60	m	k_{88}	5.14×10^6	N/m
h_2	10.00	m	k_{89}	-1.77×10^8	N
h_3	20.00	m	k_{99}	8.50×10^9	N m
s	2.50	m	k_0	8.70×10^8	N m/rad
Ω	1.27	rad/s	ζ_2	0.005	—
m_0	1.70×10^4	kg	ζ_8	0.01	—
m_1	2.80×10^3	kg	ζ_9	0.01	—
m_2	1.30×10^3	kg	μ	0.01	—
m_3	1.17×10^5	kg m	H_s	2.00	m
m_{88}	1.05×10^5	kg	T_p	6.00	s
m_{89}	-1.76×10^6	kg m	ρ	1.25	kg/m ³
m_{99}	3.65×10^7	kg m ²	ρ_w	1000	kg/m ³
J_r	3.68×10^7	kg m ²	C_d	1.20	—
J_g	5.30×10^2	kg m ²	C_m	2.00	—
M_0	2.98×10^5	kg	D	6.00	m

Table 2. Results obtained from the 13-DOF model and FAST.

Item	13-DOF			FAST		
1st flap-wise frequency (HZ)	0.669			0.668		
1st edgewise frequency (HZ)	1.062			1.079		
1st tower fore-aft frequency (Hz)	0.280			0.280		
1st tower lateral frequency (Hz)	0.280			0.280		
Mean Wind Speed (m/s)	11.4	15	20	11.4	15	20
Collective pitch angle (degrees)	0.40	10.17	17.24	0.00	10.20	17.50
flap-wise tip displacement (m)	5.70	2.77	1.22	5.65	2.75	1.20
tower fore-aft displacement (m)	0.35	0.21	0.16	0.40	0.20	0.15
tower lateral displacement (m)	−0.06	−0.06	−0.06	−0.06	−0.06	−0.06

Based on the the model described in Section 2.4, the rotational sampled turbulence field has been generated. Figure 6 shows the Fourier amplitude spectrum obtained by FFT (fast Fourier transformation) of the sample curves of the rotational sampled turbulence, at the middle point of Blade 1. A very clear $1P$ (1.267 rad/s) frequency component of the turbulence in the x_2 direction can be observed in Figure 6b. Less obviously from Figure 6a, the $1P$ peak can still be observed in the turbulence acting on the blade in the x_1 direction. Figure 7 shows the influence of aeroelasticity on tower vibrations in the case of a gear-driven wind turbine with gear ratio N equal to 97. It is seen that the aerodynamic damping almost completely removes the dynamic response of the fore-aft tower vibration $q_7(t)$, while the lateral tower vibration $q_8(t)$ is almost unaffected by aerodynamic damping, justifying the necessity of implementing active vibration control algorithms in this direction.

Figure 6. Fourier amplitude spectrum of the sample curves of the rotational sampled turbulence, at the middle point of Blade 1. $V_0 = 15$ m/s, $I = 10\%$. (a) The moving frame component of the rotational sampled turbulence in the x_1 direction. (b) The moving frame component of the rotational sampled turbulence in the x_2 direction.

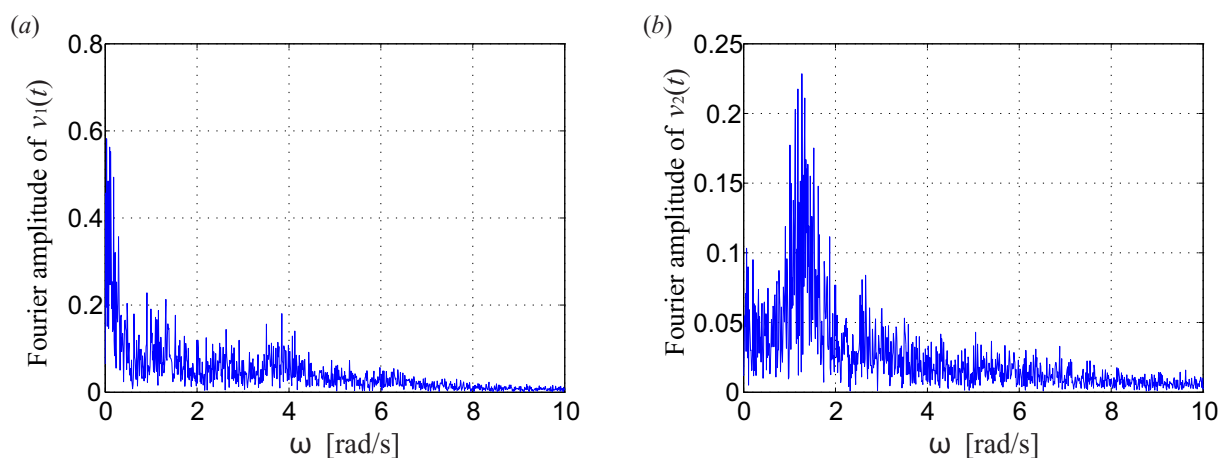
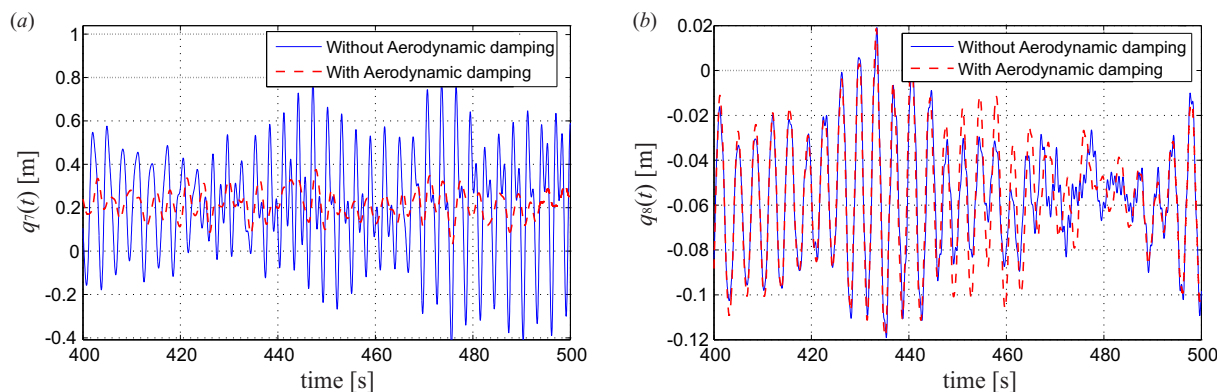


Figure 7. Tower responses with and without aerodynamic damping, gear-driven wind turbine. **(a)** Fore-aft tower top displacement. **(b)** Lateral tower top displacement. Blue curve: aerodynamic damping not considered. Red curve: aerodynamic damping considered.



Normally, in an irregular sea-state, the mean wind direction and the mean direction of wave propagation are correlated. Hence, the wave loads and the turbulent wind loads on the structure tend to be somewhat unidirectional in most cases. However, we are focusing on the lightly damped lateral tower vibration rather than the along-wind response of the tower with relatively strong aerodynamic damping. Thus, the most conservative load combination is considered in this study, *i.e.*, the wave loads are acting on the tower in the lateral direction perpendicular to the mean wind velocity, in order to fully excite the lateral tower vibration. There is also a clear physical explanation for this load combination. Due to the relatively shallow water, the waves are occasionally refracted tending to propagate orthogonal to the level curves of the sea bottom, meaning that sometimes the direction of wave propagation may take place orthogonal to the mean wind velocity. This load scenario is not expected to take place as often as the unidirectional case. However, considering an offshore wind farm with many wind turbines, there is a high chance that at all times there is a certain amount of wind turbines under such a scenario. The related parameter values used in the aerodynamic and wave loads simulation are also listed in Table 1. In [29], wave measurements were carried out at the German North Sea coast, where the water depth is 29 m. During a severe storm surge on 2 October 2009, the measured significant height was 5.23 m. This data to some extent justify the significant wave height we use ($H_s = 2$ m) for the 20-m water depth in the simulations. Extensive load cases with different combinations of V_0 and H_s (correlated with each other) are not considered in the present study.

4.2. Gear-Driven Wind Turbine

Firstly, simulations are performed considering a gear-driven wind turbine with gear ratio $N = 97$, which is in accordance with the NREL 5-MW wind turbine. In this case, the rotational speed of the generator is almost N times that of the rotor, and the magnitude of the generator torque is reduced by N times comparing with the aerodynamic torque acting at the rotor. The performance of the wind turbine system is almost the same whether the number of gear stages is odd or even, as long as the gear ratio N is unchanged. Therefore, only the results of the wind turbine with odd-numbered gear stages are illustrated.

By setting the weighting factor $W = 0.5$, meaning the same importance is placed on mitigating the tower vibration, and keeping the smoothness of the power output, the gain factor c_a is determined as

$c_a = 2.0 \times 10^4$ Ns in order to minimize the performance criterion $J(c_a)$ in Equation (22). The following figures compare the performance of the wind turbine system with the basic controller and with the active generator controller. Figure 8 shows the lateral tower top displacements $q_8(t)$ in both the time and frequency domain, where the blue line denotes the responses without active generator control and the red line with active generator control. There is a reduction of 17.8% in the maximum responses and a reduction of 37.6% in the standard deviations. For both cases, the same static displacement equal to -0.057 m is observed. This is caused by the mean value of the tower torque, which is equal to the negative mean value of the aerodynamic torque at the rotor, *i.e.*, $E[f_9(t)] = -E[f_{12}(t)]$, as explained by Equation (11). The FFT of the response $q_8(t)$ is presented in Figure 8b. For a system without active generator control, a clear peak corresponding to the tower eigenfrequency (around 1.76 rad/s) is observed without other visible peaks, owing to the fact that very low aerodynamic damping takes place in this mode. This peak is reduced to approximately $\frac{1}{3}$ by the active generator torque due to the introduced damping matrix in Equation (25). Further, it is observed that base moment of the tower in lateral direction is effectively suppressed, as well, with the standard deviation reduced from 5.12×10^6 to 3.32×10^6 Nm and the maximum value reduced from 19.63×10^6 to 15.40×10^6 Nm. The stress at the tower base in the lateral direction is calculated accordingly. There is a reduction of 35.2% (6.80 to 4.41 Mpa) in the standard deviation and a reduction of 21.6% (26.07 to 20.44 Mpa) in the maximum response, which means the fatigue lives of the tower and the foundation are effectively increased by active control.

Figure 8. Lateral tower vibration with and without active generator control, gear-driven, $W = 0.5$. (a) Time history in 400–500 s. (b) Fourier amplitude of lateral tower vibration.

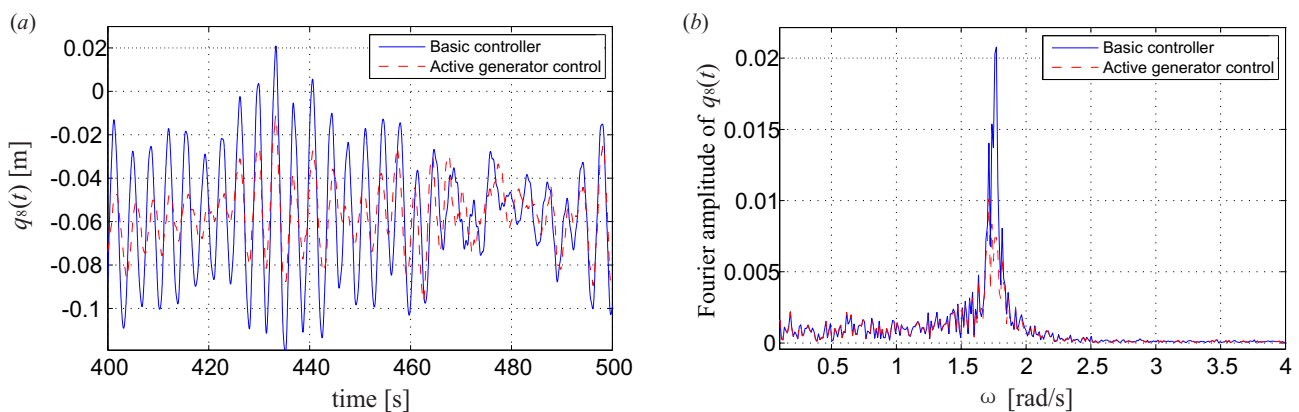
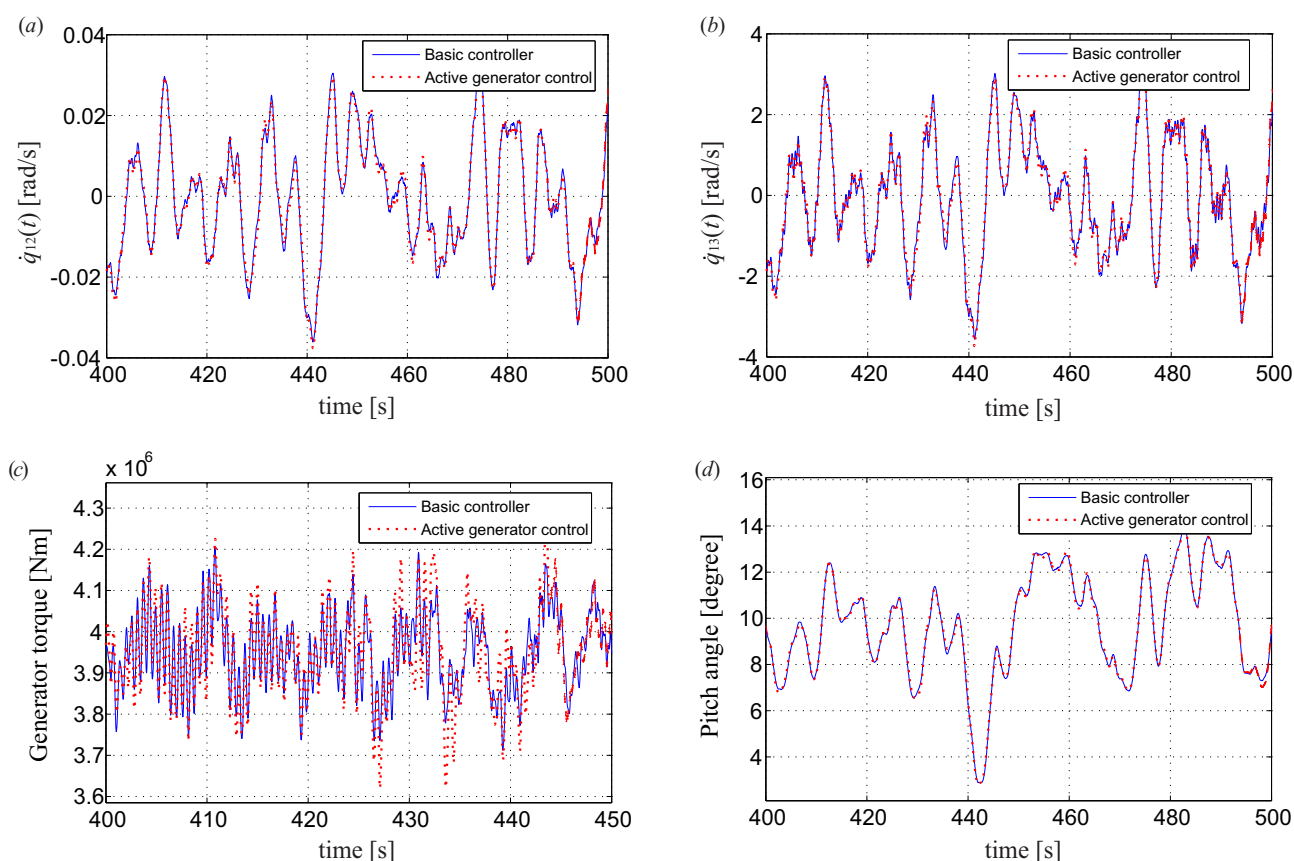


Figure 9 shows the impact of the active control on the performance of the drivetrain shafts, the gearbox and the collective pitch controller. The deviations of the rotational speed at the rotor $\dot{q}_{12}(t)$ and at the generator $\dot{q}_{13}(t)$ are very slightly affected with the standard deviations increased by 1.0% and 0.92%, respectively, reflecting a very weak coupling between the torsional vibration of the drivetrain with the lateral tower vibration. Based on Equation (13), the dynamic torque acting at the gearbox can also be obtained from $q_{12}(t)$ and $q_{13}(t)$, as shown in Figure 9c. It is seen that the active generator controller introduces a frequency component corresponding to the tower frequency in the gearbox torque, and a little more fluctuated torque is observed with an increase of 12.6% in the standard deviation, which is unfavorable for the fatigue life of the gearbox. By reducing the controller gain c_a , the negative effect can be diminished. Further, the performance of the pitch controller is almost unaffected by the

active generator control (Figure 9d) with the standard deviation increased by 0.93%. It is observed from Figure 10a,b that the flap-wise tip displacement $q_1(t)$ and tower fore-aft top displacement $q_7(t)$ are also insignificantly affected with the standard deviations increased by 0.85% and 2.2% after the implementation of active generator control. This is expected, since there is no direct coupling between these two modes of vibration with the generator torque and the lateral tower vibration. The coupling is indirectly via the pitch controller performance, which changes the effective angle of attack and the corresponding aerodynamic loads on the blade sections. Figure 10c shows an interesting result that the edgewise vibration $q_4(t)$ is slightly suppressed by the active generator control due to the coupling of edgewise vibration to the lateral tower vibration, as shown in Equation (6). The maximum response and the standard deviation are reduced by 5.5% and 5.0%, respectively. Although the focus is to control the lateral tower vibration through active generator torque, it is favorable to see that the edgewise vibration with very low aerodynamic damping is also suppressed a little, rather than being negatively affected.

Figure 9. Influence of the active generator control on the drivetrain, the gearbox and the pitch controller, gear-driven, $W = 0.5$. (a) Deviation of rotational speed of the rotor. (b) Deviation of rotational speed of the generator. (c) Torque on the gearbox. (d) Collective pitch angle.



The time history of power output from the generator is presented in Figure 11. Since the generated power is related to the lift forces along the blade and, hence, the longitudinal turbulence, the resulting power output also presents periodicity around $1P$ frequency, similarly with that in Figure 6a. Due to the torque increment $c_a \dot{q}_8(t)$, the generated power becomes more fluctuated with an increase of 1.3% in the maximum value and an increase of 33.0% in the standard deviation, relative to the values without active generator control. Since the stiffness and mass of the tower for the offshore wind turbine is very large,

it is inevitable that effective control of the tower vibration is at the expense of a little more fluctuated power output, which is unfavorable for the grid side. One possible solution to accommodate this problem is to increase the energy storage in the power converter by increasing the size of the capacitor in Figure 5. To give more clear insight into the tradeoff between the structural vibration and the power output, five different values of weighting factor W are used, *i.e.*, W is chosen to be 0.1, 0.3, 0.5, 0.7 and 0.9. For each W , an optimal value of c_a can be obtained through the optimization procedure given by Equation (22). Table 3 presents the optimized c_a and the corresponding standard deviations of $q_8(t)$ and the power output in different cases. It is shown that as the value of W increases, allowing larger values in the control effort, better structural performance, but worse power quality are achieved. For the extreme case of $W = 0.9$, the standard deviation of the lateral tower vibration can be reduced by 60%, but the fluctuation of the power output is increased by 121.7%. In this case, one solution may be to turn on the active generator controller merely when large lateral tower vibrations take place.

Figure 10. Influence of the active generator control on the flap-wise, fore-aft tower and edgewise vibrations, gear-driven, $W = 0.5$. (a) Flap-wise tip displacement. (b) Fore-aft tower top displacement. (c) Edgewise tip displacement.

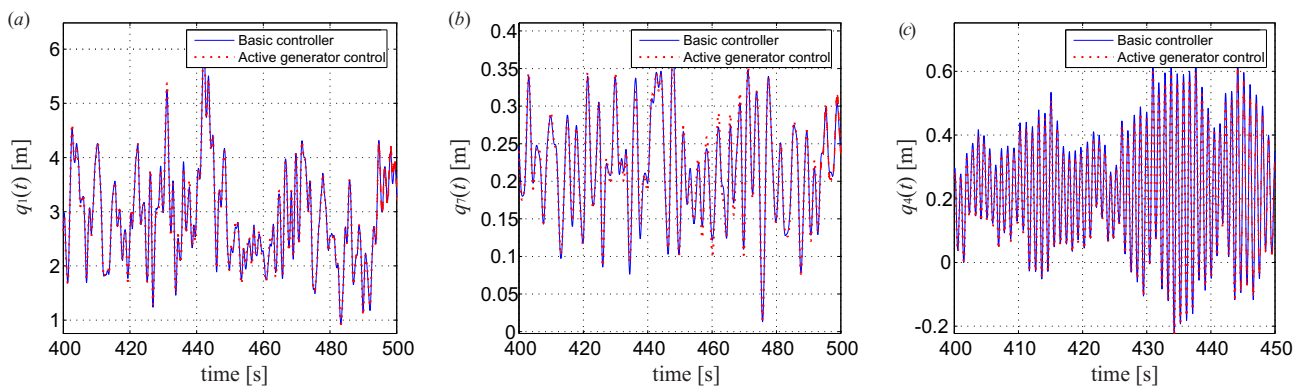


Figure 11. Time series of power output, gear-driven, $W = 0.5$.

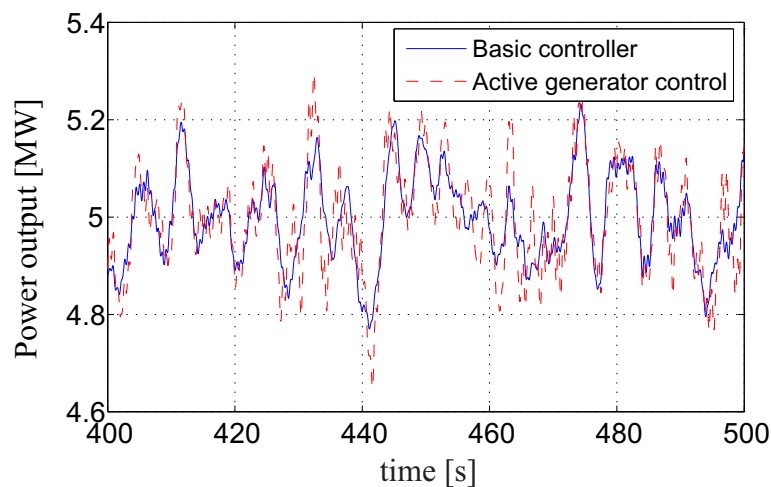


Table 3. Performance of the tower controller for the gear-driven case.

Case	c_a (Ns)	σ_{q_8} (m)	σ_P (MW)
Basic system	0	0.0330	0.106
$W = 0.1$	0	0.0330	0.106
$W = 0.3$	1.0×10^4	0.0246	0.121
$W = 0.5$	2.0×10^4	0.0206	0.141
$W = 0.7$	4.0×10^4	0.0167	0.177
$W = 0.9$	8.0×10^4	0.0132	0.235

4.3. Direct-Driven Wind Turbine

Next, simulations of the direct driven wind turbine are carried out. Comparing with the gear-driven wind turbine, the nominal generator torque is increased by N times, while the nominal rotational speed of the generator is reduced by N times. Since the magnitude of the generator is increased significantly, we take the mass moment of inertia of the generator J_g to be N times the original value in the simulation. This is justified by the data of a 3-MW wind turbine [30], where the mass moment of inertia of the generator for the direct driven wind turbine is about 150-times that of the gear-driven one (the total mass is six-times larger and the radius of the stator is five-times larger). The same turbulence field and wave loads as in the previous case are applied to the wind turbine system in order to make meaningful comparisons.

Similarly, by setting $W = 0.5$, the value of the gain factor c_a is determined as 2.0×10^6 in order to minimize the performance criterion $J(c_a)$. Figures 12–14 show the results corresponding to similar parameters studied in the previous case. Results in Figure 12 show the remarkable capability of the active generator controller in suppressing lateral tower vibrations. The maximum response of $q_8(t)$ is reduced from 0.143 to 0.105 m (reduced by 26.6%), and the standard deviation is reduced by 54.0%. Again, a static displacement equal to -0.057 m is always present with or without active control. This value is also unchanged comparing with the gear-driven case, because the mean value of the aerodynamic torque acting at the rotor is unchanged whether it is a gear-driven or direct-driven wind turbine. Further, the stress at the tower base is calculated, with the standard deviation reduced from 6.72 to 3.39 Mpa (49.6%) and the maximum response reduced from 26.12 to 18.90 Mpa (27.6%). The Fourier spectrum of the lateral tower top displacement (Figure 12b) shows that the peak around 1.76 rad/s, corresponding to the tower eigenfrequency, is almost totally eliminated by the active generator controller, comparing with that of the uncontrolled case. The reason for the superior performance is that the nominal generator torque $f_{13,0}$ is much larger in the direct-driven wind turbine, and thus, the optimized controller gain c_a , as well as the additive torque are also increased accordingly.

Figure 13 shows the impact of the active generator controller on the responses of other components of the wind turbine. Similarly, the negative influences on the drivetrain oscillation, the flap-wise vibration, the fore-aft tower vibration and the performance of the pitch controller are negligible. The lightly-damped edgewise vibration in Blade 1 ($q_4(t)$) is again slightly suppressed by the active generator control, due to its coupling to the lateral tower vibration. Similar results have been confirmed for the

other two blades. It should be noted that the gearbox is eliminated in the direct-driven system, and the negative impact from the active generator torque on the gearbox as stated in the gear-driven case is no longer a problem for the direct-driven case.

Figure 12. Lateral tower vibration with and without active generator control, direct-driven, $W = 0.5$. (a) Time history in 400–500 s. (b) Fourier amplitude of lateral tower vibration.

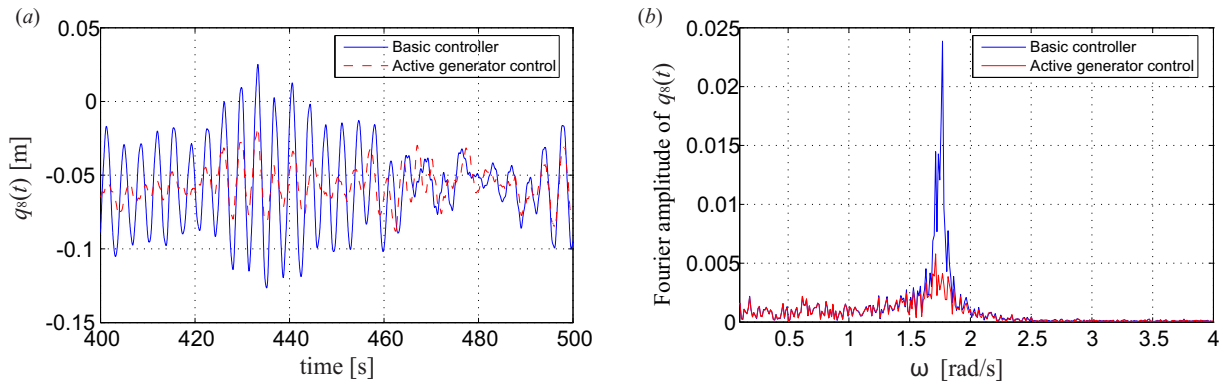


Figure 13. Influence of the active generator control on system responses, direct-driven, $W = 0.5$. (a) Deviation of rotational speed of the rotor. (b) Deviation of rotational speed of the generator. (c) Collective pitch angle. (d) Flap-wise tip displacement. (e) Fore-aft tower top displacement. (f) Edgewise tip displacement.

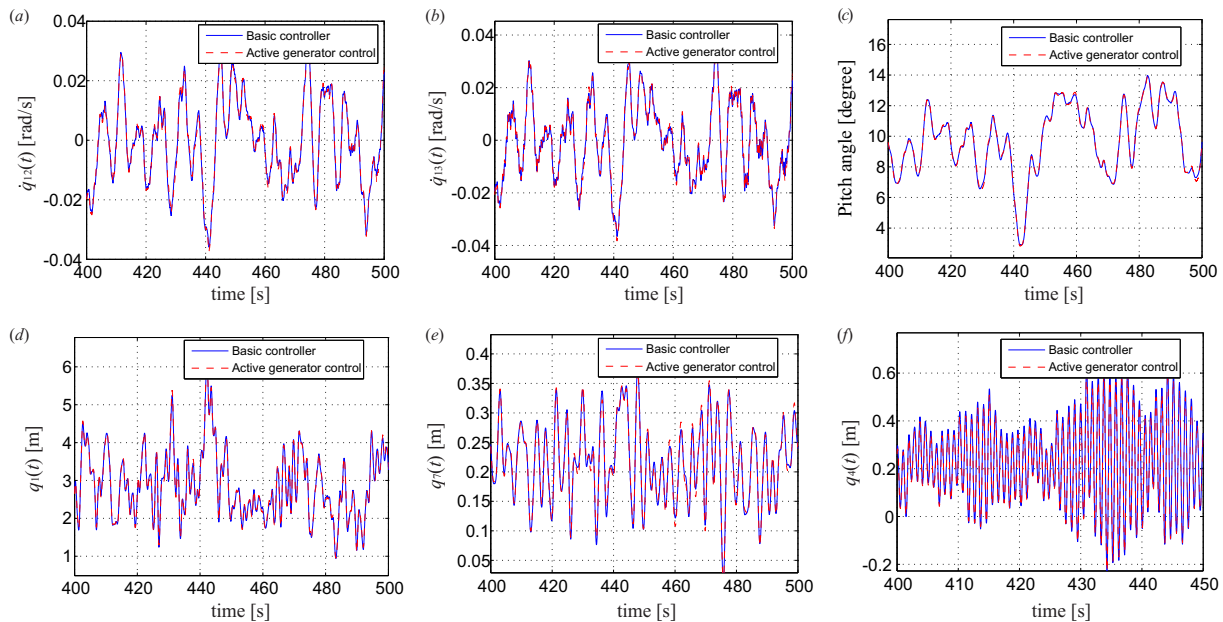


Figure 14 shows the time-history of the power output from the generator. A little negative effect on the smoothness of the power output is observed after the implementation of the active generator control. The maximum value of the power output is increased from 5.41 MW to 5.48 MW (increased by 1.3%), and the standard deviation is increased from 0.108 MW to 0.125 MW (increased by 15.7%), which means less impact on the grid side than that of the gear-driven case. For direct-driven wind turbines, the value of $f_{13,0}$ is significantly increased, and the relative magnitude between $c_a \dot{q}_8(t)$ and $f_{13,0}$ is smaller comparing with that of the gear-driven turbine; thus, the smoothness of the power output is less affected by the active

control. Similarly, the tradeoff between the tower vibration and the power output is illustrated in Table 4, showing that as the value of the weighting factor W increases, better structural performance, but worse power quality are obtained. However, acceptable results for the power quality can always be obtained when the tower vibration is significantly reduced.

Figure 14. Time series of power output, direct-driven, $W = 0.5$.

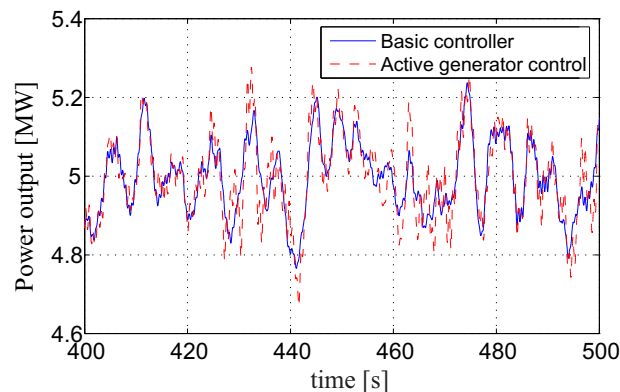


Table 4. Performance of the tower controller for the direct drive case.

Case	c_a (Ns)	σ_{q_8} (m)	σ_P (MW)
Basic system	0	0.0328	0.108
$W = 0.1$	0	0.0328	0.108
$W = 0.3$	1.0×10^6	0.0189	0.116
$W = 0.5$	2.0×10^6	0.0151	0.125
$W = 0.7$	3.0×10^6	0.0132	0.134
$W = 0.9$	8.0×10^6	0.0099	0.175

5. Conclusions

This paper presents a comprehensive investigation into the modeling and control of lateral tower vibrations of offshore wind turbines using active generator torque. A 13-DOF wind turbine model has been developed using a Euler–Lagrangian approach, taking into consideration the quasi-static nonlinear aeroelasticity. The equation of motion was derived, and the coupling of the blade-tower-drivetrain motion, as well as the load transfer mechanisms from the generator to the tower are demonstrated. A simple feedback controller was proposed for lateral tower vibrations through the active generator torque, and a generator model was introduced as the power electronic solution for providing the additive generator torque in real time.

Numerical simulations have been carried out using data calibrated to the referential 5-MW NREL offshore wind turbine. Cases of the gear-driven and the direct-driven wind turbines were both considered to evaluate the effectiveness of the active generator torque for mitigating lateral tower vibrations. The non-linear time-history results demonstrate that for both gear-driven and direct-driven wind turbines, the active generator controller is successfully able to reduce the lateral tower vibration induced by the combined aerodynamic and hydrodynamic loads. The effective control of lateral tower vibration is at the expense of a little more fluctuated power output, and a tradeoff between the vibration aspect and

the power electronic aspect should be considered by properly choosing the controller gain. The active generator controller has negligible effects on the drivetrain oscillation, the flap-wise vibration, the fore-aft tower vibration and the performance of the controller. It is also favorable to observe that the lightly-damped edgewise vibration is slightly suppressed by the active generator controller due to its coupling to the lateral tower vibration. The active generator controller shows superior performance for the direct-driven wind turbine, since a better vibration control efficacy can be obtained with less impact on the smoothness of the power output.

In further works, a more sophisticated and realistic consideration of the wind-wave correlation needs to be investigated. The controller will also be developed in more detail, such as to include filters and to design the controller when there is a slight rotor imbalance.

Acknowledgments

The first author gratefully acknowledges the financial support from the Chinese Scholarship Council under the State Scholarship Fund.

Author Contributions

This paper is a result of the collaboration of all co-authors. Zili Zhang and Søren R.K. Nielsen established the wind turbine model and designed the controller. Frede Blaabjerg and Dao Zhou proposed the power electronic solution for the active generator control. Zili Zhang was mainly responsible for numerical simulation, results interpretation and initial writing. All co-authors performed editing and reviewing of the paper.

Conflicts of Interest

The authors declare no conflict of interest.

References

1. Hansen, M.H. Aeroelastic instability problems for wind turbines. *Wind Energy* **2007**, *10*, 551–577.
2. Thomsen, K.; Petersen, J.T.; Nim, E.; Oye, S.; Petersen, B. A method for determination of damping for edgewise blade vibrations. *Wind Energy* **2000**, *3*, 233–246.
3. Murtagh, P.J.; Ghosh, A.; Basu, B.; Broderick, B.M. Passive control of wind turbine vibrations including blade/tower interaction and rotationally sampled turbulence. *Wind Energy* **2008**, *11*, 305–317.
4. Colwell, R.; Basu, B. Tuned liquid column dampers in offshore wind turbines for structural control. *Eng. Struct.* **2009**, *31*, 358–368.
5. Lackner, M.A.; Rotea, M.A. Passive structural control of offshore wind turbines. *Wind Energy* **2011**, *14*, 373–388.
6. Zhang, Z.L.; Chen, J.B.; Li, J. Theoretical study and experimental verification of vibration control of offshore wind turbines by a ball vibration absorber. *Struct. Infrastruct. Eng.* **2014**, *10*, 1087–1100.

7. Lackner, M.A.; Rotea, M.A. Structural control of floating wind turbines. *Mechatronics* **2011**, *21*, 704–719.
8. Burton, T.; Sharpe, D.; Jenkins, N.; Bossanyi, E.A. *Wind Energy Handbook*; John Wiley Sons, Ltd.: West Sussex, UK, 2001.
9. Bossanyi, E.A. Wind turbine control for load reduction. *Wind Energy* **2003**, *6*, 229–244.
10. Licari, J.; Ugalde-Loo, C.E.; Ekanayake, J.B.; Jenkins, N. Damping of torsional vibrations in a variable-speed wind turbine. *IEEE Trans. Energy Convers.* **2013**, *28*, 172–180.
11. Dixit, A.; Suryanarayanan, S. Towards pitch-scheduled drive train damping in variable-speed, horizontal-axis large wind turbines. In Proceedings of the 44th IEEE Conference on Decision and Control, and the European Control Conference 2005, Seville, Spain, 12–15 December 2005.
12. Van der Hooft, E.; Schaak, P.; van Engelen, T. *Wind Turbine Control Algorithms*; Technical Report ECN-C-03-111; Energy Research Center of the Netherlands (ECN): Petten, The Netherlands, 2003.
13. De Corcuera, A.D.; Pujana-Arrese, A.; Ezquerro, J.M.; Seguro, E.; Landaluze, J. H_∞ based control for load mitigation in wind turbines. *Energies* **2012**, *5*, 938–967.
14. Fleming, P.A.; van Wingerden, J.W.; Wright, A.D. Comparison state-space multivariable controls to multi-SISO controls for load reduction of drivetrain-coupled modes on wind turbines through field-testing. In Proceedings of 50th AIAA Aerospace Sciences Meeting, Nashville, TN, USA, 9–12 January 2012.
15. Blaabjerg, F.; Chen, Z.; Kjaer, S.B. Power electronics as efficient interface in dispersed power generation systems. *IEEE Trans. Power Electron.* **2004**, *19*, 1184–1194.
16. Jonkman, J.; Butterfield, S.; Musial, W.; Scott, G. *Definition of 5-MW Reference Wind Turbine for Offshore System Development*; Technical Report NREL/TP-500-38060; National Renewable Energy Laboratory (NREL): Golden, CO, USA, 2009.
17. Krenk, S.; Svendsen, M.N.; Høgsberg, J. Resonant vibration control of three-bladed wind turbine rotors. *AIAA J.* **2012**, *50*, 148–161.
18. Sarpkaya, T.; Isaacson, M. *Mechanics of Wave Forces on Offshore Structures*; Van Nostrand Reinhold: New York, NY, USA, 1981.
19. Ogata, K. *Morden Control Engineering*; Prentice Hall: Upper Saddle River, NJ, USA, 2009.
20. Pars, L.A. *A Treatise on Analytical Dynamics*; Ox Bow Press: Woodbridge, ON, Canada, 1979.
21. Clough, R.W.; Penzien, J. *Dynamics of Structures*; McGraw-Hill: New York, NY, USA, 1993.
22. *Wind Turbine Part 1; Design Requirements*; IEC 61400-1; International Electrotechnical Committee: Geneva, Switzerland, 2005.
23. Batchelor, G.K. *The Theory of Homogeneous Turbulence*; Cambridge University Press: Cambridge, UK, 1953.
24. Hansen, M.O.L. *Aerodynamics of Wind Turbines*; Earthscan: London, UK, 2008.
25. Hasselmann, K.; Barnett, T.P.; Bouws, E.; Carlson, H.; Cartwright, D.E.; Enke, K.; Ewing, J.A.; Gienapp, H.; Hasselmann, D.E.; Kruseman, P.; et al. *Measurement of Wind-Wave Growth and Swell Decay during the Joint North Sea Wave Project (JONSWAP)*; Deutsches Hydrographisches Institut: Hamburg, Germany, 1973.

26. Chinchilla, M.; Arnaltes, S.; Burgos, J.C. Control of permanent-magnet generators applied to variable-speed wind-energy systems connected to the grid. *IEEE Trans. Energy Convers.* **2006**, *12*, 130–135.
27. Novotny, D.W.; Lipo, T.A. *Vector Control and Dynamics of ac Drives*; Clarendon Press: Oxford, UK, 1996.
28. Jonkman, J.; Musial, W. *Offshore Code Comparison Collaboration (OC3) for IEA Task 23 Offshore Wind Technology and Deployment*; Technical Report NREL/TP-5000-48191; National Renewable Energy Laboratory (NREL): Golden, CO, USA, 2010.
29. Mai, S.; Wilhelmi, J.; Barjenbruch, U. Wave height distributions in shallow waters. *Coast. Eng. Proc.* **2010**, *32*, doi:10.9753/icce.v32.waves.63.
30. Polinder, H.; van der Pijl, F.F.A.; de Vilder, G.-J.; Tavner, P.J. Comparison of direct-drive and geared generator concepts for wind turbines. *IEEE Trans. Energy Convers.* **2006**, *21*, 725–733.

© 2014 by the authors; licensee MDPI, Basel, Switzerland. This article is an open access article distributed under the terms and conditions of the Creative Commons Attribution license (<http://creativecommons.org/licenses/by/4.0/>).